

RESEARCH

Open Access



# Impact of *POU3F4* mutation on cochlear development and auditory function

Jiong Dang<sup>1†</sup>, Panpan Bian<sup>1†</sup>, Chao Chen<sup>2†</sup>, Chi Chen<sup>1</sup>, Wenqi Shan<sup>2</sup>, Luhang Cai<sup>2</sup>, Yong Li<sup>1</sup>, Huan Tan<sup>1</sup>, Baicheng Xu<sup>1\*†</sup>, Minxin Guan<sup>2\*†</sup> and Yufen Guo<sup>1\*†</sup>

## Abstract

**Background** Hearing loss, a major public health issue, affects 1.33 per 1,000 live births worldwide. Genetic factors contribute to over half of congenital cases, with X-linked inheritance accounting for 1–5%. *POU3F4* mutations are associated with approximately 50% of X-linked non-syndrome hearing loss cases. *POU3F4* plays a critical role in cochlear development by regulating otic mesenchyme cell differentiation. The study investigates the impact of a novel *POU3F4* p.E294G mutation on cochlear structure and function using cellular and animal model.

**Methods** The study utilized immortalized lymphoblastoid cell lines, *POU3F4* overexpressed HEK293 cells and generated *Pou3f4* knock-in (*Pou3f4KI*) mice via CRISPR/Cas9 to introduce the p.E294G mutation. Alterations in expression and subcellular localization of *POU3F4* were detected at the cellular level. Auditory function was assessed using auditory brainstem response testing. Cochlear structure was analyzed through histology, immunohistochemistry, scanning electron microscopy, and transmission electron microscopy. RNA sequencing, qPCR and Western blot were conducted to evaluate gene expression and mitochondrial function.

**Results** The transcription of *POU3F4* was abnormal and the expression was normal in lymphoblastoid cell lines. Abnormal nuclear localization of *POU3F4* p.E294G was found in overexpressed HEK293 cells. *Pou3f4KI* mice exhibited cochlear malformations, including modiolus hypoplasia and reduced stria vascularis cell populations. Auditory testing revealed progressive hearing loss. *Pou3f4* affect mitochondrial protein expression by affecting the expression of TFAM. Mitochondrial dysfunction was evident, with reduced oxidative phosphorylation (OXPHOS) complex assembly and activity, decreased ATP levels. The level of reactive oxygen species, mitochondrial fission and apoptosis in cochlea were elevated.

<sup>†</sup>Jiong Dang, Panpan Bian and Chao Chen contributed equally to this work and should be regarded as co-first authors.

<sup>†</sup>Yufen Guo, Minxin Guan and Baicheng Xu contributed equally to this work and should be regarded as co-corresponding authors.

\*Correspondence:

Baicheng Xu  
xbsuc@126.com  
Minxin Guan  
gminxin88@zju.edu.cn  
Yufen Guo  
guoyflz@163.com

Full list of author information is available at the end of the article



© The Author(s) 2025. **Open Access** This article is licensed under a Creative Commons Attribution-NonCommercial-NoDerivatives 4.0 International License, which permits any non-commercial use, sharing, distribution and reproduction in any medium or format, as long as you give appropriate credit to the original author(s) and the source, provide a link to the Creative Commons licence, and indicate if you modified the licensed material. You do not have permission under this licence to share adapted material derived from this article or parts of it. The images or other third party material in this article are included in the article's Creative Commons licence, unless indicated otherwise in a credit line to the material. If material is not included in the article's Creative Commons licence and your intended use is not permitted by statutory regulation or exceeds the permitted use, you will need to obtain permission directly from the copyright holder. To view a copy of this licence, visit <http://creativecommons.org/licenses/by-nc-nd/4.0/>.

**Conclusions** The *POU3F4* p.E294G resulted in abnormal nuclear localization. *Pou3f4* mutant disrupts cochlear development and function, impairs mitochondrial integrity, induces oxidative stress, and promotes apoptosis, leading to progressive hearing loss. The findings enhance the understanding of *POU3F4*-related hearing loss mechanisms and highlight the importance of early genetic screening and audiological monitoring.

**Keywords** *POU3F4*, Cochlear development, Hearing loss, Mitochondrial dysfunction, Apoptosis, Oxidative phosphorylation, Cochlear malformations

## Background

Hearing loss affects millions globally and is a significant public health concern, impacting about 1.33 per 1,000 live births, increasing through childhood to adolescence [1–3]. Genetic factors are responsible for more than half of congenital hearing loss cases, with X-linked inheritance accounting for 1–5% globally [4, 5]. Among these, *POU3F4* mutations are implicated in about 50% of X-linked non-syndromic hearing loss cases, making it a crucial target for further research [6].

*POU3F4* encodes a neural transcription factor of the POU Class III family, primarily involved in inner ear development [7]. Mutations in *POU3F4* are linked to mixed deafness, characterized by incomplete partition type 3 (IP-3), stapes fixation, and cerebrospinal fluid gusher during surgery [7–9]. Its primary function involves regulating otic mesenchyme cells (OMCs) differentiation, which are essential for proper cochlear development [10].

The role of *POU3F4* in cochlear development remain unclear. Only a few potential transcriptional targets, such as *EPHA4* and *EFNB2*, have been identified, but direct binding sites and downstream effects are still poorly understood [10, 11]. *POU3F4* is expressed in various cochlear cell types, including OMCs in embryo and spiral ligament fibrocytes (SLFs) and spiral limbus, modiolar osteoblasts, specialized tympanic border cells of the basilar membrane and basal cells of the stria vascularis differentiate from OMCs, indicating its broad role in maintaining cochlear structural integrity [12]. Given the critical role of *POU3F4* in cochlear development and the gaps in understanding its molecular targets and mechanisms, this study aims to elucidate the impact of a novel *POU3F4* mutation on cochlear structure and function, using cell model and animal model. This study focuses on the *POU3F4* p.E294G mutation, located within the highly conserved POU-homeo domain. Given its potential to alter transcription factor activity, understanding its effect could provide key insights into the pathology of *POU3F4*-related hearing loss.

## Materials and methods

### Protein structure prediction for *POU3F4* c.881 a>g mutation

To predict the structural effects of the *POU3F4* c.881 A>G mutation, we first retrieved the wild-type

protein sequence from the UniProt database. We then utilized homology modeling tools, such as SWISS-MODEL, to generate three-dimensional models for both the wild-type and mutant proteins. After obtaining the models, we performed energy minimization to optimize their structures. The predicted structures were visualized using PyMOL to assess conformational differences between the wild-type and mutant proteins. This analysis provided insights into how the c.881 A>G mutation might affect the protein's structure and potential function.

### Cell lines and culture conditions

Immortalized lymphoblastoid cell lines were generated from family members (II-1, II-2, III-1 and III-2), and named the cell lines heterozygote (Het), wild-type, hemizygote1 (Hemi1) and hemizygote2 (Hemi2) respectively [13]. These cell lines were cultured in RPMI 1640 medium with 10% fetal bovine serum (FBS).

### Plasmid construction and cell transduction

The HEK293 cells were cultured in Dulbecco's Modified Eagle Medium (DMEM) (Gibco), supplemented with 10% FBS. *POU3F4*-wild-type (*POU3F4*-WT) and c.881 A>G mutation (*POU3F4*-MUT) expression plasmids were constructed by cloning the respective binding sites into the p-EGFP-N1 vector. Cell lines were transfected at 70–80% confluence in 6-well plates using jetPRIME (Polyplus), according to the manufacturer's instructions. After 48 h, the samples were collected.

### Generation of the *Pou3f4*KI mouse

All procedures involving animals were coincided with animal ethics and were approved by the Animal Care and Use Committees of the Lanzhou University. The gRNA to mouse *Pou3f4* (p.E294G) gene, the donor oligo containing p.E294G (GAA to GGA) mutation and two synonymous mutations (p.L293= (CTG to CTC) and p.L298= (CTC to TTG)), and Cas9 were co-injected into fertilized mouse eggs to generate targeted knock in offspring (Supplement Figure 1). gRNA target sequence: gRNA-A1 (matching forward strand of gene): GGTGAGTGTC AAGGGCGTACTGG and gRNA-A2 (matching reverse strand of gene): CTGCAGGCTTGGGACACTTGAG G.F0 founder animals were identified by PCR followed by sequence analysis, which were bred to wildtype mice

to test germline transmission and F1 animal generation. For the genotypic analysis, total DNA was extracted from the tails of pups and confirmed by Sanger sequencing genomic DNA from exon 1 using primers flanking the site of the mutation: F: 5'-AAAGAAGAATCAAGTTGG GCTTCAC-3' and R: 5'-CTAGCAAGCTAGAGAGATA GCAAC-3'.

#### Auditory brainstem response (ABR)

ABR recording experiments were performed as detailed elsewhere [14]. ABR thresholds were recorded to assess the hearing of mice. Pou3f4KI and WT mice were anesthetized by intraperitoneal injection of Tribromoethanol (0.2mL/10 g) and their body temperature was maintained at 37°C. The evoked brainstem response to click and pure tones (4, 8, 16, 24, 32 kHz) was measured. The SPL from 90 to 20 dB in a 5 dB ~ 10 dB step and the lowest dB SPL level at which the ABR pattern could be recognized was

defined as the ABR threshold. The Tucker-Davis Technologies workstation provided the auditory stimulation, signal reception, and amplification; the coupled BioSigRZ software was used to analyze data.

#### Immunofluorescence staining

Cochlea tissues were fixed in 4% paraformaldehyde (PFA) for 48 h, decalcified with EDTA for 48 h, and then dehydrated using a graded ethanol series. Tissues were embedded in paraffin, and 10 µm thick sections were cut. Sections were deparaffinized with a series of xylene and ethanol washes and followed by blocking with 5% bovine serum albumin (BSA) in PBS for 1 h at room temperature. Sections were incubated with primary antibodies (see Table 1) at 4 °C overnight. After washing with PBS, sections were incubated with fluorophore-conjugated secondary antibodies (see Table 1) for 1 h, protected from light. Sections were stained with DAPI to label cell nuclei. Fluorescence images were acquired using a Leica microscope, Zeiss LSM880 confocal laser scanning microscope, or TissueFAXS Plus quantitative imaging system.

#### Hematoxylin and Eosin (HE) staining

Tissue sections were processed as described for immunofluorescence, with deparaffinization and rehydration through graded ethanol solutions. Sections were stained with hematoxylin solution for 1 min, followed by washing with PBS. They were then stained with eosin for 2 min.

#### Scanning electron microscopy (SEM)

Freshly isolated cochleae were locally perfused through oval and round windows with 2.5% glutaraldehyde in phosphate buffer (0.1 M, pH 7.4) fixed overnight at 4°C. Cochlear surface of the adult mouse prepared as previously described [15]. Samples were fixed with 1% osmium solution for 1.5 h and rinsed with PBS. Samples were dehydrated through a graded series of ethanol (50%, 70%, 90% and 100%) and dried by Critical Point Dryer CPD 300 (Leica). Dried specimens were sputter coated with Pt-palladium (8 mA, 60s) by high vacuum ion sputtering apparatus (Quorum Q150T ES plus) and observed with a scanning electron microscope Nova Nano 450 (Thermo FEI) at 5kv.

#### Transmission electron microscopy (TEM)

Cochlear fixation and cochlear surface prepared as previously described in SEM. Sample prepared as previously described [16]. Electron photomicrographs were taken from ultrastructure of cells under a transmission electron microscopy (Hitachi, H-7650).

#### Western blot

Cells and Mouse cochleae were homogenized in RIPA buffer (Beyotime) containing 1mM complete protease

**Table 1** Antibody reagents list for experimental studies

Antibody	Source	Identifier
Rabbit monoclonal anti-β-Actin	Abclonal	Cat#AC038
Rabbit Polyclonal anti-POU3F4	Proteintech	Cat#25114-1-AP
Mouse Monoclonal anti-TUJ1	Proteintech	Cat# 66375-1-Ig
Rabbit Polyclonal anti-Myosin VIIa/MYO7A	Abcam	Cat#ab150386
Rabbit polyclonal anti-NDUFA10	Abclonal	Cat#A10123
Rabbit polyclonal anti-OPA1	Abclonal	Cat#A9833
HRP-labeled goat anti-rabbit IgG	Beyotime	Cat#A0208
HRP-labeled goat anti-mouse IgG	Beyotime	Cat#A0216
Rabbit monoclonal anti-CASP7	Cell Signaling	Cat#12,827
Rabbit polyclonal anti-BCL-XL	Cell Signaling	Cat#2762
Mouse monoclonal anti-CYTC	Proteintech	Cat#66264-1-Ig
Mouse monoclonal anti-MFF	Proteintech	Cat#66527-1-Ig
Rabbit polyclonal anti-ATP5A1	Proteintech	Cat#14676-1-AP
Rabbit polyclonal anti-BAD	Proteintech	Cat#10435-1-AP
Rabbit polyclonal anti-BAX	Proteintech	Cat#50599-2-Ig
Rabbit polyclonal anti-CASP3/P17/P19	Proteintech	Cat#19677-1-AP
Rabbit polyclonal anti-CASP9/P35/P10	Proteintech	Cat#10380-1-AP
Rabbit polyclonal anti-COX5A	Proteintech	Cat#11448-1-AP
Rabbit polyclonal anti-DRP1	Proteintech	Cat#12957-1-AP
Rabbit polyclonal anti-FIS1	Proteintech	Cat#10956-1-AP
Rabbit polyclonal anti-MFN1	Proteintech	Cat#13798-1-AP
Rabbit polyclonal anti-MFN2	Proteintech	Cat#12186-1-AP
Rabbit polyclonal anti-NDUFS1	Proteintech	Cat#18443-1-AP
Rabbit polyclonal anti-SDHB	Proteintech	Cat#10620-1-AP
Rabbit polyclonal anti-UQCRF51	Proteintech	Cat#18443-1-AP
Alexa Fluor 488 goat anti-mouse IgG	Thermofisher	Cat#A21202
Alexa Fluor 488 goat anti-rabbit IgG	Thermofisher	Cat#A11008
Alexa Fluor 594 goat anti-rabbit IgG	Thermofisher	Cat#A11012

inhibitor cocktail (Selleckchem) and incubated for 30 min on ice. The lysates were cleared by centrifugation, and the total protein concentration was determined using a BCA assay kit (Beyotime) according to the manufacturer's instructions. Protein samples were mixed with 5× SDS-PAGE loading buffer and boiled at 95 °C for 5 min. A total of 25 µg protein was loaded onto 12% bis-Tris SDS-polyacrylamide gels for electrophoresis. Proteins were transferred to PVDF membranes using a wet transfer system. Membranes were blocked in PBST (PBS with 0.1% Tween-20) containing 5% dry milk and incubated with primary antibodies overnight at 4 °C. The primary antibodies (listed in Table 1) were diluted in PBST containing 5% BSA. After washing, membranes were incubated with HRP-conjugated secondary antibodies (Goat Anti-Mouse IgG(H+L) or Goat Anti-Rabbit IgG(H+L), Beyotime) for 2 h at room temperature. Protein signals were detected using the ECL system (CW BIO).

#### Reverse transcription and quantitative PCR

Total RNA was extracted from the cell samples and cochlea samples using the FreeZol Reagent (Vazyme) according to the manufacturer's instructions. The RNA concentration of the samples was determined using a NanoDrop2000 spectrophotometer (Thermo Fisher Scientific). cDNA synthesis was performed using the HiScript II Q Select RT SuperMix for qPCR(+gDNA wiper) (Vazyme). qPCR was performed with primers: F: GCAG GTTCGAGGCCTTACAA, R: AGTACGCCCTTGAC ACTCAC. Real-time PCR analysis was performed using Hieff qPCR SYBR Green Master Mix (Yeasen) in FQD-96 A Real-Time PCR system instrument (Bioer) to determine the expression levels of genes. Data processing as previously described [17].

#### RNA sequencing (RNA-seq) analysis

Total RNA was extracted from the cochlea of 3 month old WT and Pou3f4KI mice using TRIzol reagent (Thermo Fisher) according to the manufacturer's protocol. RNA quality was assessed using NanoDrop and Bioanalyzer (Agilent), and samples with concentration >50 ng/µl, RIN >7.0, and >1 µg total RNA were used for library preparation. Poly(A)+mRNA was isolated using oligo(dT) magnetic beads (Thermo Fisher), fragmented with NEBNext® Magnesium RNA Fragmentation Module (NEB) at 94 °C for 5–7 min, and reverse transcribed into cDNA using SuperScript II Reverse Transcriptase (Invitrogen). cDNA libraries were prepared with the NEBNext® Ultra™ RNA Library Prep Kit for Illumina® (NEB) and amplified by PCR. The libraries were sequenced on an Illumina NovaSeq 6000 platform (LC Bio Technology) in paired-end mode (PE150). Raw data were processed to obtain clean reads, which were aligned to the mouse reference genome (Ensembl release 97) using TopHat

(version 2.1.0). Differential gene expression was analyzed using Cufflinks (version 2.2.1).

#### Mitochondria isolation from mouse cochleae

Freshly dissected mouse cochleae were minced and resuspended in 6 volumes of mitochondria isolation buffer (75mM sucrose, 225mM D-mannitol, 30mM Tris-HCl, pH 7.4) supplemented with protease inhibitor cocktail and 1mM PMSF. The tissue was homogenized on ice using a Dounce homogenizer. The homogenate was centrifuged at 1000 rpm for 5 min at 4 °C twice, and the supernatant was collected. Following this, the supernatant was centrifuged at 13,000 rpm for 15 min at 4 °C to pellet the mitochondria. The mitochondrial pellet was carefully resuspended in 100 µL of isolation buffer. The protein concentration of the isolated mitochondria was determined using the BCA protein assay. For further analysis, mitochondria were aliquoted at 400 µg per tube and stored at –80 °C.

#### Blue-native PAGE analysis

For membrane protein extraction, mitochondria were resuspended in 20% digitonin (w/v) on ice for 20 min. After digitonin treatment, the sample was centrifuged at 20,000 rpm for 20 min at 4 °C, and the supernatant was collected for further analysis. The protein concentration was again determined by the BCA assay. Samples containing 30 µg of total mitochondrial proteins mixed were separated on 3–12% Bis-Tris Native PAGE gel. The complex activity assays described previously [18]. Gels were scanned to visualize the activities of respiratory chain complexes. Detection of multiprotein complexes subunits by immunoblotting was performed as described previously [19].

#### Quantification and statistical analysis

All statistical analyses were performed using GraphPad Prism (version 9.00) for statistical analysis to compare outcomes using a two-tailed unpaired Student's t test. *p* values of less than 0.05 were considered to be statistically significant.

## Results

### Clinical characterization

A Dongxiang nationality family (Fig. 1A) was identified through the infant hearing screening program at the Otolaryngology Clinic of Second Affiliated Hospital of Lanzhou University, China. The proband (III-1) exhibited profound sensorineural hearing loss by the age of 2, as confirmed by ABR and auditory steady-state response (ASSR) testing (Fig. 1B). III-2 was also affected, initially showing profound sensorineural hearing loss at six months of age. Interestingly, his hearing partially improved by the age of 1, with ABR and ASSR showing

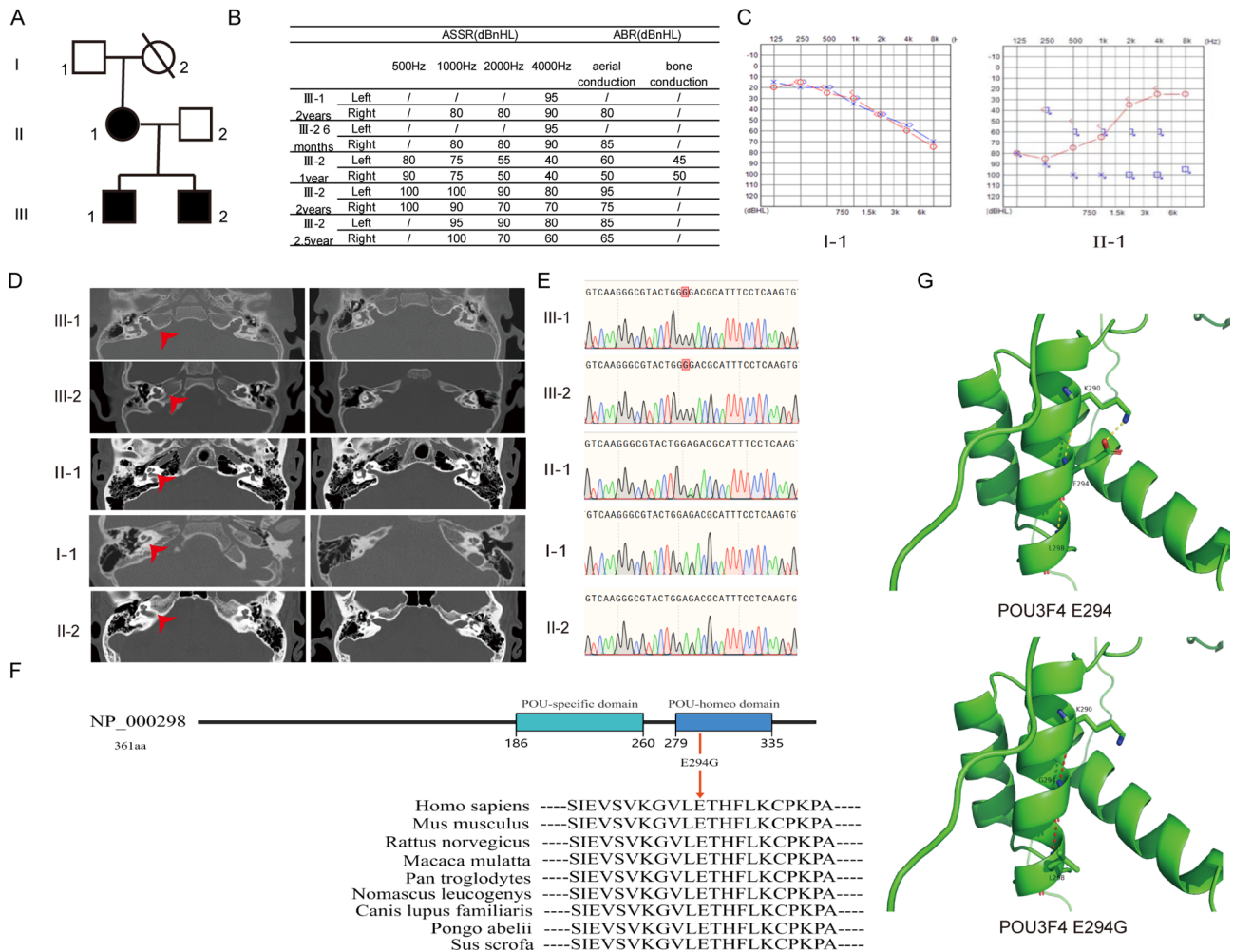


**Fig. 1** Clinical Characterization and Identification of *POU3F4* p.E294G Mutation. **(A)** Pedigree chart of a Dongxiang nationality family affected by sensorineural hearing loss. **(B)** Auditory brainstem response (ABR) and auditory steady-state response (ASSR) results showing the hearing loss profiles of the proband (III-1) and his brother (III-2). Progressive and fluctuating hearing loss patterns were noted in both individuals. **(C)** Audiometric profiles of family members, including the mother (II-1) and grandfather (I-1), indicating varying severities of hearing loss. **(D)** High-resolution axial CT scans revealing cochlear malformations, including dilated lateral ends of the internal auditory meatus and incomplete basal cochlear turns (IP-3) in affected family members. **(E)** Sanger sequencing confirms the presence of the novel *POU3F4* p.E294G mutation (c.881 A > G) in hemizygous form in the proband and his brother and in heterozygous form in their mother. **(F)** Cross-species conservation analysis highlights the critical functional importance of the Glu residue at position 294 in the *POU3F4* protein. **(G)** Predicted structural model of the *POU3F4* p.E294G mutation illustrating the disruption of key hydrogen bonds in the POU-homeo domain, likely destabilizing its conformation

mid-to-high frequency moderate sensorineural in the right ear and mixed hearing loss in the left ear, alongside profound bilateral low frequency sensorineural hearing loss. However, his hearing deteriorated again by the age of 2.5, resulting in profound sensorineural hearing loss in the left ear and severe sensorineural hearing loss in the right ear (Fig. 1B). II-1 had profound sensorineural hearing loss in the left ear and low-to-mid frequency severe mix hearing loss in the right ear at the age of 30 (Fig. 1C). I-1 experienced bilateral high-frequency sensorineural deafness, considered age-related hearing loss (Fig. 1C). None of the family members exhibited other clinical abnormalities, such as muscular diseases, vision impairment, or neurological issues, nor had they been

exposed to ototoxic drugs or excessive noise. High-resolution axial CT (HRCT) revealed distinct anatomical features. The proband (III-1) and III-2 exhibited dilation of the lateral ends of the internal auditory meatus, along with incomplete basal cochlear turns, also known as IP-3. By contrast, the HRCT of II-1 showed a widened internal auditory canal, while I-1 and II-2 displayed normal cochlear morphology (Fig. 1D).

**Identification of the mutation of *POU3F4* gene**

Based on previous literature reports, we found that IP-3 malformations are associated with *POU3F4*, so we performed full-length sequencing of *POU3F4* in the proband (III-1). After performing full-length sequencing of

*POU3F4*, we identified *POU3F4* c.881 A>G mutation in the proband (III-1). Sanger sequencing revealed III-1 and III-2 had the hemizygous mutation. II-1 was a heterozygous carrier, and I-1 and II-2 was unaffected (Fig. 1E). These results are consistent with the family cosegregation pattern. The glutamic acid (Glu) residue at position 294 in the *POU3F4* protein is highly conserved across multiple species, including *Homo sapiens*, *Mus musculus*, and *Pan troglodytes*, among others, indicating its functional importance (Fig. 1F). Based on in silico predictions and population variant frequencies, the *POU3F4* p.E294G mutation is likely pathogenic. Protein structure prediction indicated that this mutation likely results in the substitution of Glu for glycine (Gly) at position 294, disrupting hydrogen bonding with adjacent residues, such as K290 and L298, destabilizing the POU-homeo domain (Fig. 1G).

#### *POU3F4* expression in immortalized lymphocyte lines

We constructed a family-derived immortalized lymphoid cell line (ILCL) by collecting peripheral blood from family members (II-2, II-1, III-1 and III-2) to establish the WT, Het, Hemi1 and Hemi2 cell lines, respectively. To further evaluate the effect of c.881 A>G mutation on ILCL, we performed qPCR analysis of *POU3F4* using total RNA isolated from WT, Het, Hemi1 and Hemi2 as templates. As shown in Fig. 2A, the results revealed that the hemizygous mutation c.881 A>G affect the stability of *POU3F4* mRNA and alter its transcription. We

performed Western blot to assess the effect of *POU3F4* c.881 A>G mutation on ILCL differentiation. As shown in Fig. 2B and D, the results showed no significant changes in protein expression.

#### Mutation alters *POU3F4* protein localization and expression

To experimentally test the predicted effect of the mutation on *POU3F4*, we used p-EGFP-N1 as a vector, constructed *POU3F4* wild-type (*POU3F4*-WT) and c.881 A>G mutation (*POU3F4*-MUT) binding site expression plasmids and transfected them and unloaded plasmid (Vector) into HEK293 cells. As shown in Figures 2C and E, the proteins were extracted and analyzed by Western blot. The results revealed that overexpression of c.881 A>G caused a loss of the *POU3F4* protein.

To determine whether any of the pathogenic effects of mutations in this study are due to abnormal subcellular localization, we examined the subcellular localization of each mutant protein. Immunohistochemical staining revealed that the effect of *POU3F4* c.881 A>G mutation on subcellular localization (Fig. 2F). *POU3F4*-WT localized to the nucleus. However, in *POU3F4*-MUT, the majority of the *POU3F4* protein was located in the cytoplasm. *POU3F4* c.881 A>G affect the subcellular localization of *POU3F4* protein.

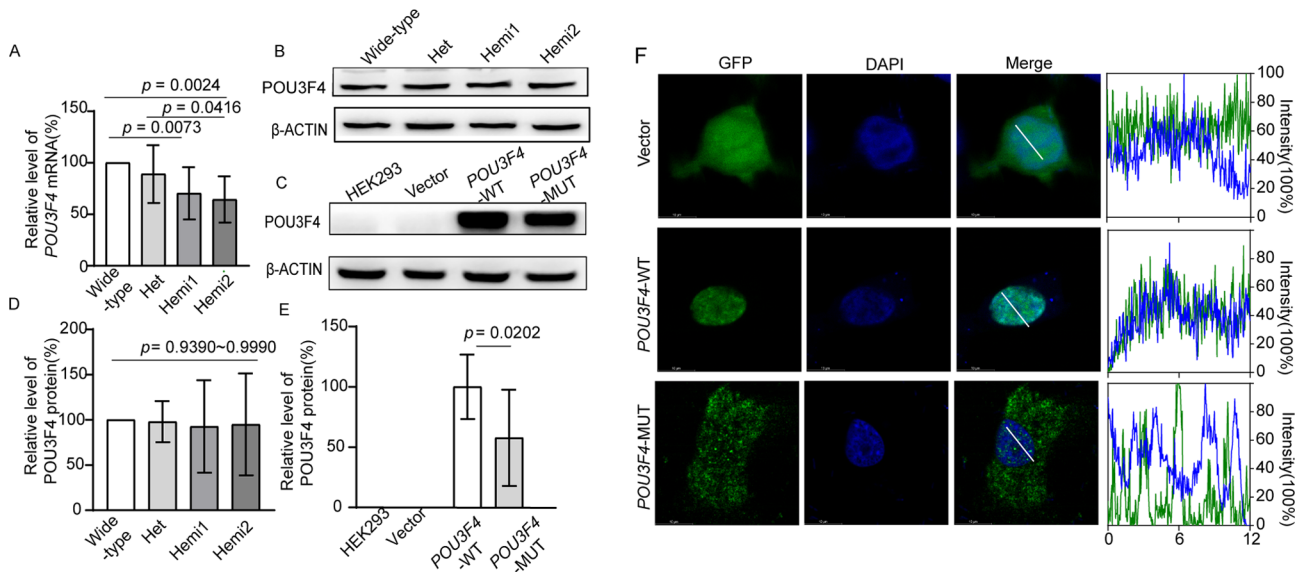


**Fig. 2** Effects of c.881 A > G Mutation on *POU3F4* Expression and Intracellular Localization. **(A)** qPCR analysis shows that the c.881 A > G mutation affects *POU3F4* mRNA stability and transcription levels in immortalized lymphocyte lines (WT, Het, Hemi1, and Hemi2). **(B, D)** Western blot analysis reveals no significant changes in *POU3F4* protein expression in the lymphocyte lines, suggesting that transcriptional changes may not directly impact protein levels under these conditions. **(C, E)** Transfection of HEK293 cells with WT or MUT *POU3F4* constructs demonstrates that the c.881 A > G mutation leads to a significant loss of *POU3F4* protein expression. **(F)** Immunohistochemical staining shows a distinct subcellular localization of *POU3F4*. In *POU3F4*-WT, *POU3F4* predominantly localizes to the nucleus, while in *POU3F4*-MUT, it is mislocalized to the cytoplasm, indicating that the c.881 A > G mutation disrupts normal nuclear targeting of the protein

### Generation and characterization of Pou3f4KI mice

To investigate the role of the *POU3F4* p.E294G mutation in auditory dysfunction, we generated Pou3f4KI mice using CRISPR/Cas9 in the CBA/6J genetic background. The gRNA targeting the *Pou3f4* gene was designed to introduce the p.E294G mutation, along with two synonymous mutations at p.L293 and p.L298. Following the injection of gRNA, donor oligonucleotides, and Cas9 into fertilized mouse eggs, founder animals were identified via PCR and Sanger sequencing, confirming successful incorporation of the mutation (Supplement Fig. 1A and B).

### Expression analysis of Pou3f4 in mice model

To further characterize the impact of the mutation on *Pou3f4* expression, we performed RT-qPCR and Western blot analysis on cochlear tissues. The RT-qPCR results indicated a 60% reduction in *Pou3f4* mRNA levels in Pou3f4KI mice compared to WT controls ( $p < 0.001$ , Fig. 3A). Similarly, Western blot analysis revealed a significant 70% decrease in POU3F4 protein levels in the cochlea of Pou3f4KI mice at P28 ( $p < 0.0001$ , Fig. 3B and C).

### Auditory function assessment in Pou3f4KI mice

Auditory function was evaluated using ABR testing at postnatal days 14, 28, and 84 (P14, P28, and P84). At P14, all Pou3f4KI mice exhibited undetectable hearing, indicating delayed auditory development compared to WT controls. At P28, a small subset of Pou3f4KI mice showed minimal hearing improvement, with slightly lower ABR thresholds. However, by P84, all mutants exhibited significantly elevated ABR thresholds, which eventually progressed to complete hearing loss (Fig. 3D and E F). These findings reflect variability in auditory phenotypes, consistent with the clinical heterogeneity observed in human cases of the *POU3F4* p.E294G mutation. Alteration in Morphology of the Cochlea in Pou3f4KI Mice.

HE staining of mid-modiolar cochlear sections revealed several dysplastic features in the cochleae of Pou3f4KI mice. Notable malformations observed in the cochlea included hypoplasia of the modiolus, reduction in the size of the tympanic scala, and apparent cell loss in the stria vascularis, spiral ligament, and spiral limbus (Fig. 4A).

SEM images revealed notable morphological changes in the cochlea of Pou3f4KI mice. The stereocilia of outer hair cells showed transposition, with a reduction in the number of outer hair cells and inner hair cells, as well as the interconnecting filamentous bridges. Additionally,

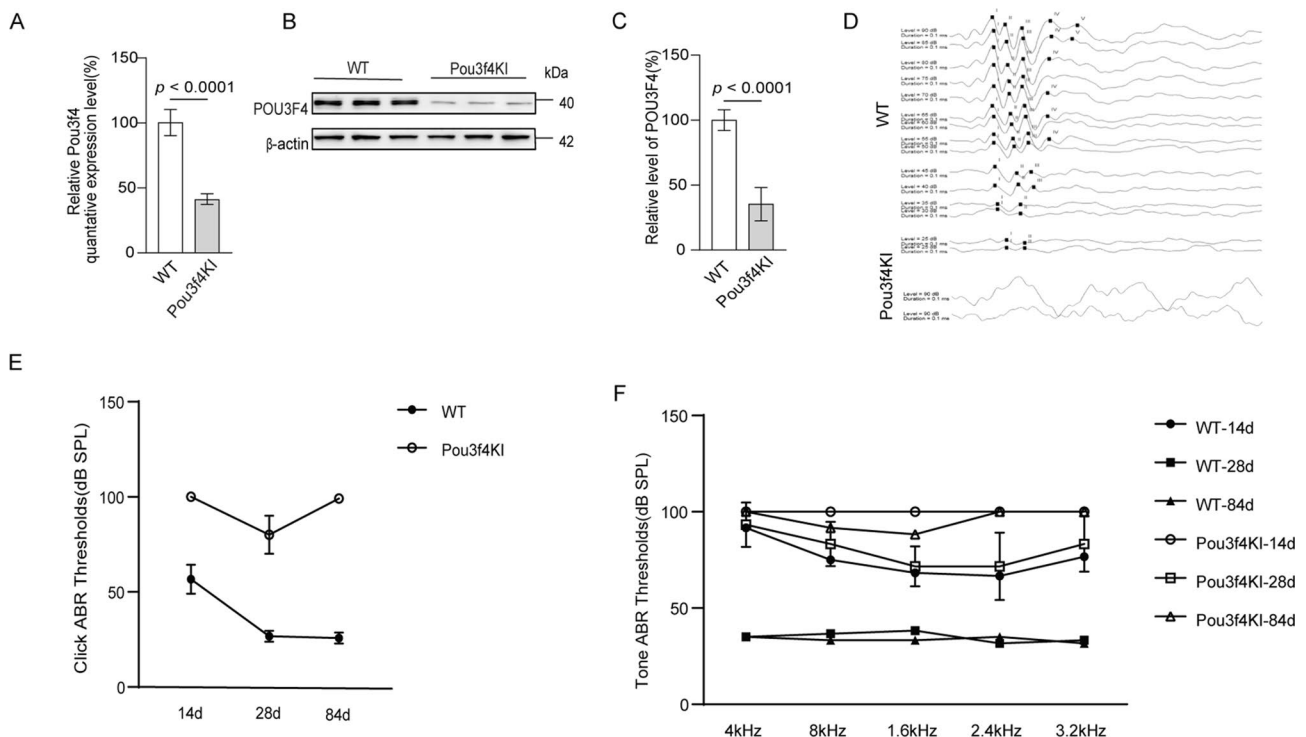


**Fig. 3** Generation and Characterization of Pou3f4KI Mice with p.E294G Mutation. (A–C) Expression analysis in Pou3f4KI mice: RT-qPCR reveals a 60% reduction in *Pou3f4* mRNA levels, and Western blot shows a 70% decrease in POU3F4 protein levels in cochlear tissues compared to WT controls, confirming the impact of the p.E294G mutation. (D–F) Auditory brainstem response (ABR) testing indicates delayed auditory development at P14, partial hearing recovery at P28, and progressive hearing loss culminating in complete deafness by P84 in Pou3f4KI mice

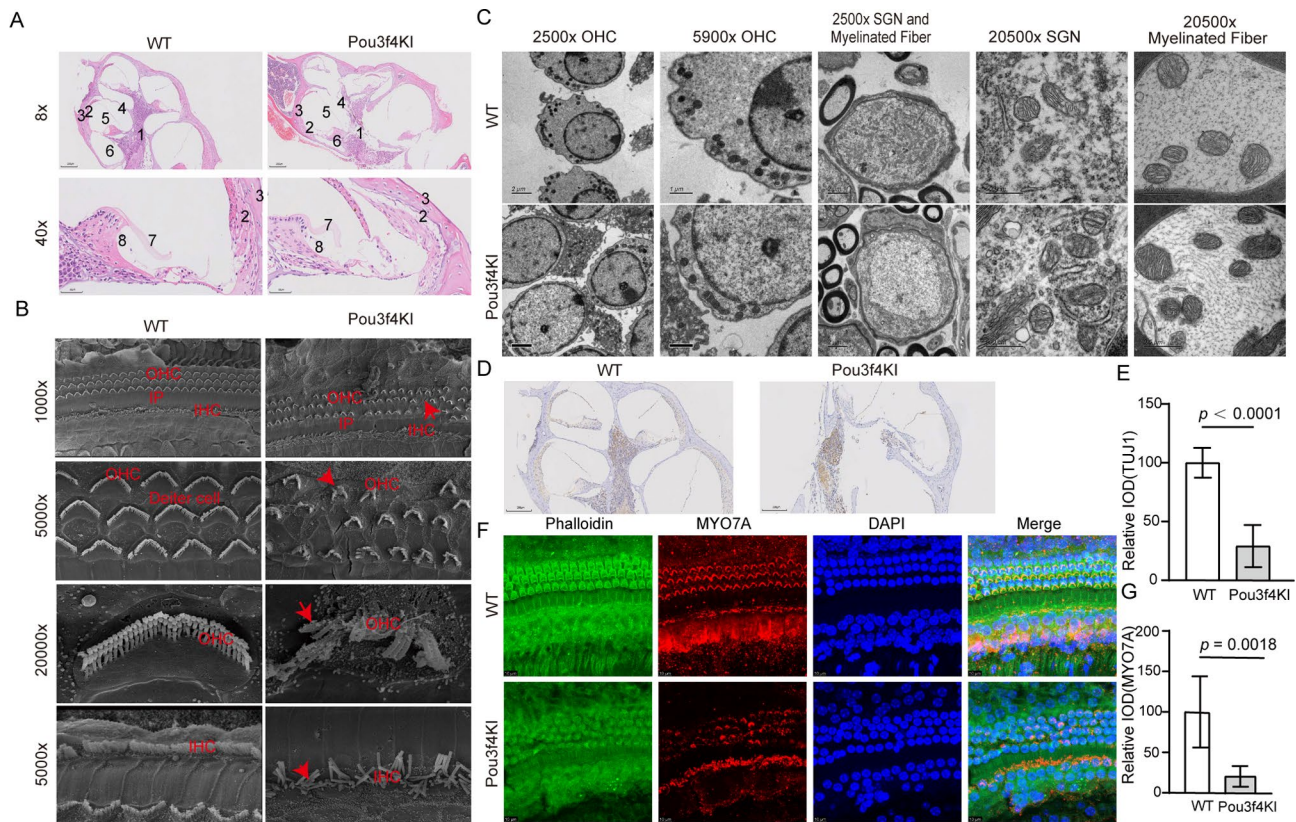


**Fig. 4** Cochlear Structural and Cellular Abnormalities in *Pou3f4KI* Mice. **(A)** Hematoxylin and eosin (HE) staining highlights cochlear malformations, including modiolus hypoplasia, reduced tympanic scala size, and cell loss in the stria vascularis, spiral ligament, and spiral limbus. **(B)** Scanning electron microscopy (SEM) images show morphological abnormalities, including dislodged stereocilia and reduced numbers of both inner and outer hair cells with disrupted interconnecting bridges. **(C)** Transmission electron microscopy (TEM) demonstrates mitochondrial abnormalities in spiral ganglion neurons (SGNs) and myelinated fibers, including swelling, deformation, and loss of membranes and cristae. **(D-G)** Immunostaining for Tuj1 and MYO7A reveals significant reductions in SGNs (70%) and hair cells (79%) in *Pou3f4KI* mice compared to WT, particularly in critical regions such as the basilar membrane

the stereocilia of both outer and inner hair cells appeared dislodged (Fig. 4B).

TEM images demonstrated that most of the mitochondria in the spiral ganglion neurons (SGNs) and myelinated fibers were abnormal. These abnormalities included swollen and deformed mitochondria, characterized by the loss of membranes and inner cristae (Fig. 4C).

#### Loss of SGNs and hair cells in *Pou3f4KI* cochleae

Immunostaining for Tuj1 and MYO7A revealed a significant reduction in both SGNs and hair cells in *Pou3f4KI* mice compared to WT controls. Specifically, Tuj1 staining demonstrated a reduction of approximately 70% in relative integrated optical density (IOD) in the basilar membrane ( $p < 0.0001$ , Figures S1C and S1D) and an overall decrease in SGNs throughout the cochlea, with IHC for Tuj1 further confirming a nearly 50% decrease in relative IOD ( $p < 0.0001$ , Fig. 4D and E). MYO7A, a marker for hair cells, showed a marked decrease in expression in the organ of Corti in *Pou3f4KI* cochleae, with the relative IOD reduced by approximately 79% ( $p = 0.0018$ , Fig. 4F and G). These results indicate that

the *Pou3f4* mutation leads to a loss of both hair cells and SGNs, particularly in regions critical for cochlear function, such as the basilar membrane.

#### Transcriptome changes of the cochlea in *Pou3f4KI* mice

To investigate the effects of *Pou3f4* mutations on cochlear gene expression, RNA-seq was performed on cochlear samples from *Pou3f4KI* and WT mice. A total of 3,279 differentially expressed genes (DEGs) were identified with criteria of  $FDR \leq 0.05$  and  $|\log_2FC| \geq 1$ . Among these, 1,650 genes were upregulated and 1,629 were downregulated in *Pou3f4KI* mice compared to WT controls. The results are presented in a volcano plot (Fig. 5A).

Gene set enrichment analysis (GSEA) revealed significant alterations in multiple biological pathways in *Pou3f4KI* mice compared to WT controls. Gene Ontology (GO) enrichment analysis showed that biological processes, including apoptosis and calcium signaling, were up-regulated, whereas pathways related to the mitochondrial function were down-regulated (Fig. 5B). Similar changes were found in Kyoto Encyclopedia of Genes and Genomes (KEGG) enrichment analysis (Fig. 5C).



Among the mitochondrial genes, 13 genes were upregulated and 121 were downregulated in *Pou3f4*KI mice compared to WT controls. The results are presented in a heatmap (Fig. 5D).

#### Investigating POU3F4-regulated pathways via POU2F1 and POU5F1 CHIP-seq

Considering mitochondrial abnormalities observed in *Pou3f4*KI mice via TEM and downregulated mitochondrial pathways revealed by transcriptomic data, we investigated POU3F4's impact on mitochondrial function. POU2F1, POU5F1 and POU3F4 share a conserved DNA-binding motif, "TATGCAAT" (Fig. 5E) [20]. ChIP-seq data for POU2F1 and POU5F1, obtained from the ENCODE database [21], allowed us to perform an in-depth regulatory analysis. ChIP-seq revealed a prominent POU2F1 and POU5F1 binding peak within the TFAM promoter, suggesting that these transcription factors may regulate TFAM expression (Fig. 5F). To investigate whether TFAM is influenced by POU3F4, we performed Western blot analysis to measure TFAM protein levels in cochlear samples from WT and *Pou3f4*KI mice. The TFAM levels in *Pou3f4*KI cochleae were reduced to 54% ( $p=0.0028$ ) of those in WT cochleae (Fig. 5G and H). In HEK293 cells, TFAM expression levels were 11.2% higher in the *POU3F4*-WT group compared to the untransfected HEK293 group ( $p=0.0023$ ) and 40% higher than in the Vector group ( $p=0.0152$ ). In contrast, TFAM expression was 19.2% lower in the *POU3F4*-WT group compared to the *POU3F4*-MUT group ( $p=0.0417$ ). No significant differences were observed in TFAM expression among untransfected HEK293 cells, Vector and *POU3F4*-MUT groups. (Figure 5I and J).

#### Reduced levels of nDNA- and mtDNA-encoded mitochondrial OXPHOS proteins

To evaluate the impact of the *Pou3f4* c.881 A>G mutation on mitochondrial OXPHOS proteins, Western blot analysis was performed to quantify the levels of 19 subunits from OXPHOS complexes in the cochleae of WT and *Pou3f4*KI mice. The analysis showed significant reductions in 16 out of 19 mitochondrial proteins in *Pou3f4*KI mice, compared to WT mice. Specifically, levels of ND1, ND3, ND5, ND6, CYTB, CO1, ATP6, ATP8, NDUFS1, NDUFA8, NDUFA10, NDUFA11, UQCRCF1, and COX5A in *Pou3f4*KI cochleae were reduced to 40%, 68%, 47%, 67%, 52%, 73%, 52%, 26%, 60%, 61%, 72%, 60%, 51%, and 54% of those in WT cochleae, respectively. However, the levels of CO2, SDHA, SDHB, UQCRH and ATP5A1 remained unchanged between the two groups (Fig. 6A, B and C).

#### Reduction of the activity and assembly of mitochondrial complexes

OXPHOS complex assembly and activity were analyzed using blue native polyacrylamide gel electrophoresis (BN-PAGE) and Western blot. Impaired assembly of complexes I, III, IV, and V was observed in *Pou3f4*KI cochleae compared to WT controls. Quantitative analysis showed significant reductions in the levels of complexes I, III, IV, and V, which were reduced to approximately 57%, 54%, 74%, and 43% of WT levels, respectively, while complex II levels remained unchanged (Fig. 6D and E). Consistently, in-gel activity assays revealed impaired activities of complexes I, IV, and V, showing reductions of 37%, 17%, and 54%, respectively, compared to WT, with complex II activity showing no detectable changes (Fig. 6F and J).

#### Significant reduction of ATP levels in *Pou3f4*KI cochleae

The ATP levels in the cochleae of *Pou3f4*KI mice were significantly reduced compared to WT mice, showing a 74% decrease (Fig. 6H). This reduction indicates a substantial impairment in cochlear energy metabolism in *Pou3f4*KI mice.

#### Enhanced the production of mitochondrial ROS

To further assess whether the *Pou3f4* c.881 A>G mutation-induced mitochondrial ROS production affected the antioxidant systems, we examined the levels of SOD2, SOD1 and CATALASE in cochlea of the *Pou3f4*KI mice. As shown in Fig. 7A and B, the cochleae of *Pou3f4*KI mice revealed marked increases in the levels of CATALASE (180%), SOD1 (140%) and SOD2 (127%), respectively.

#### Imbalanced mitochondrial dynamics

To evaluate whether the *Pou3f4* c.881 A>G mutation affected the mitochondrial dynamics, we examined mitochondrial fission and fusion in the cochleae of *Pou3f4*KI mice and WT mice by Western blot analyses. As shown in Fig. 7C and D, the levels of three fusion-related proteins (MFN1, MFN2, and OPA1) and three fission-related proteins (DRP1, FIS1, and MFF) in cochlea of the *Pou3f4*KI mice and WT mice were assessed by Western blot analysis. The average level of DRP1, FIS1, and MFF in cochlea of *Pou3f4*KI mice were 221%, 154%, and 242% of the average values measured in cochlea of WT mice, respectively. In contrast, the average level of OPA1 in cochlea of *Pou3f4*KI mice were 38% of the mean values measured in cochlea of WT mice. However, the average level of MFN1 and MFN2 in the cochlea of *Pou3f4*KI mice were comparable to those in WT mice.

#### Increased apoptosis in *Pou3f4*KI mice cochleae

TUNEL staining revealed a significant increase in apoptotic cells in the cochleae of *Pou3f4*KI mice compared to WT controls. The relative IOD of TUNEL-positive cells

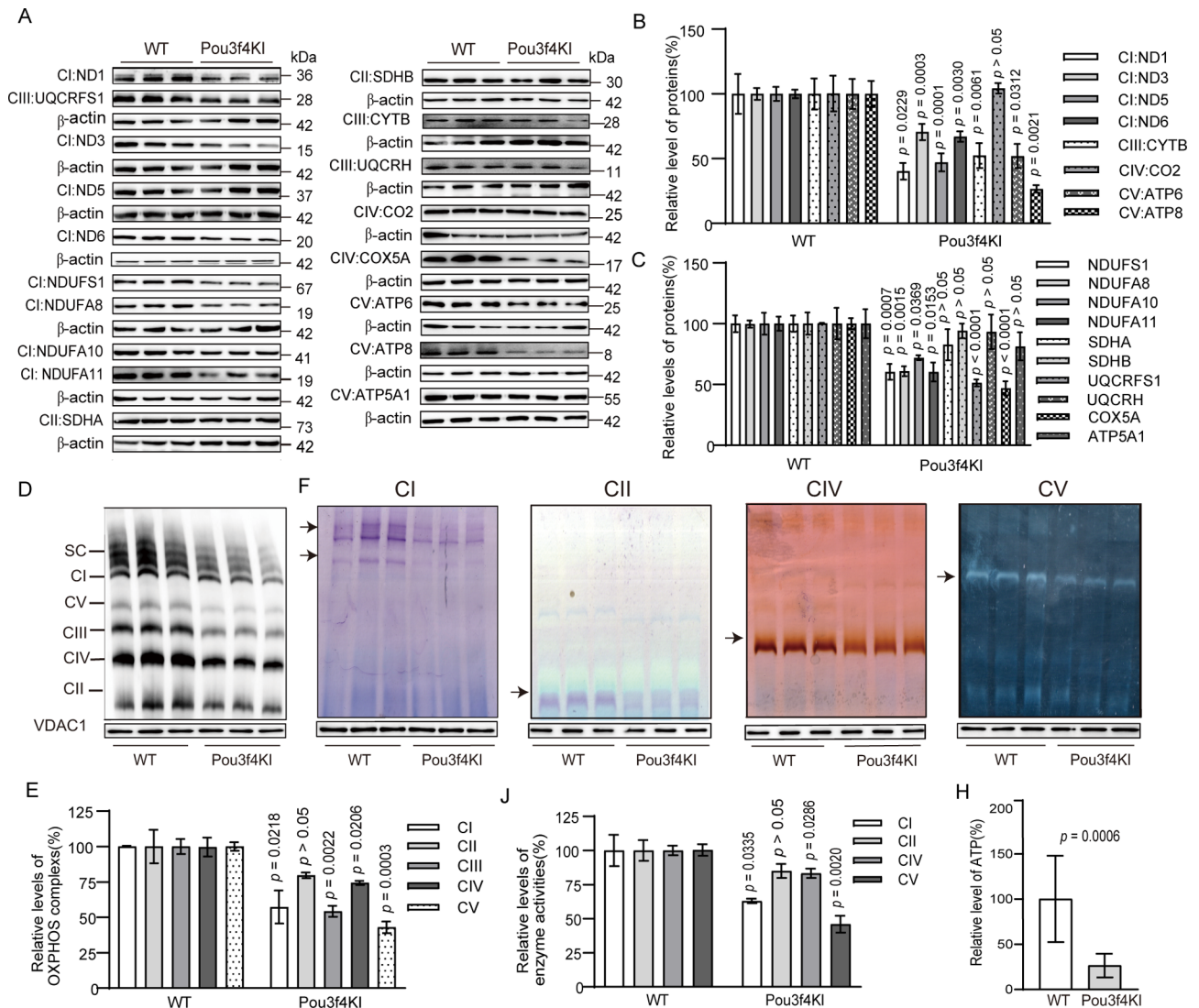


**Fig. 6** Mitochondrial OXPHOS Protein Defects and Energy Imbalance **(A, B)** Western blot analysis of mitochondrial OXPHOS proteins shows significant reductions in 16 out of 20 subunits in Pou3f4KI cochleae, affecting complexes I, III, IV, and V, while levels of complexes II subunits remain unchanged. **(D, E)** Blue native PAGE (BN-PAGE) reveals impaired assembly of OXPHOS complexes I, III, IV, and V, with assembly reduced to 57%, 54%, 74%, and 43%, respectively, compared to WT. **(F, J)** In-gel activity assays confirm functional defects in complexes I, IV, and V, with activity reductions to 63%, 83%, and 46%, respectively. **(H)** ATP quantification reveals a 67.5% reduction in ATP levels in Pou3f4KI cochleae compared to WT, indicating severe energy metabolism disruption

in Pou3f4KI cochleae was approximately 3.1 times higher than in WT ( $p=0.0008$ , Fig. 7E and F). This increase in apoptosis was predominantly localized to the SGNs, hair cells, spiral ligament, spiral limbus, modiolus, striae vasculosa and basilar membrane.

Mitochondrial fission machinery actively participates in the process of intrinsic apoptosis. To examine the impact of *Pou3f4* c.881 A>G mutation-induced fission on apoptosis, we performed Western blot assays. We assessed the levels of two apoptosis inhibited protein (BCL-XL, BCL-2) and seven activated proteins (Cytochrome C, BAD, BAX, CASPASES3, 7 and 9, and C-CASPASE9) in the cochleae of Pou3f4KI and WT

mice by Western blot analysis. As shown in Fig. 7J and H, the average levels of BCL-XL, BCL-2, Cytochrome C, BAD, BAX, CASPASES 3, 7 and 9, and C-CASPASE9 in the cochlea of Pou3f4KI mice were 63%, 66%, 159%, 178%, 178%, 121%, 199%, 139% and 182% of the mean values measured in WT mice, respectively. These results strongly indicated that the *Pou3f4* c.881 A>G mutation promoted apoptotic process.

### Discussion

This study identifies a novel *POU3F4* p.E294G mutation that significantly impacts cochlear development and hearing function. By integrating clinical observations,

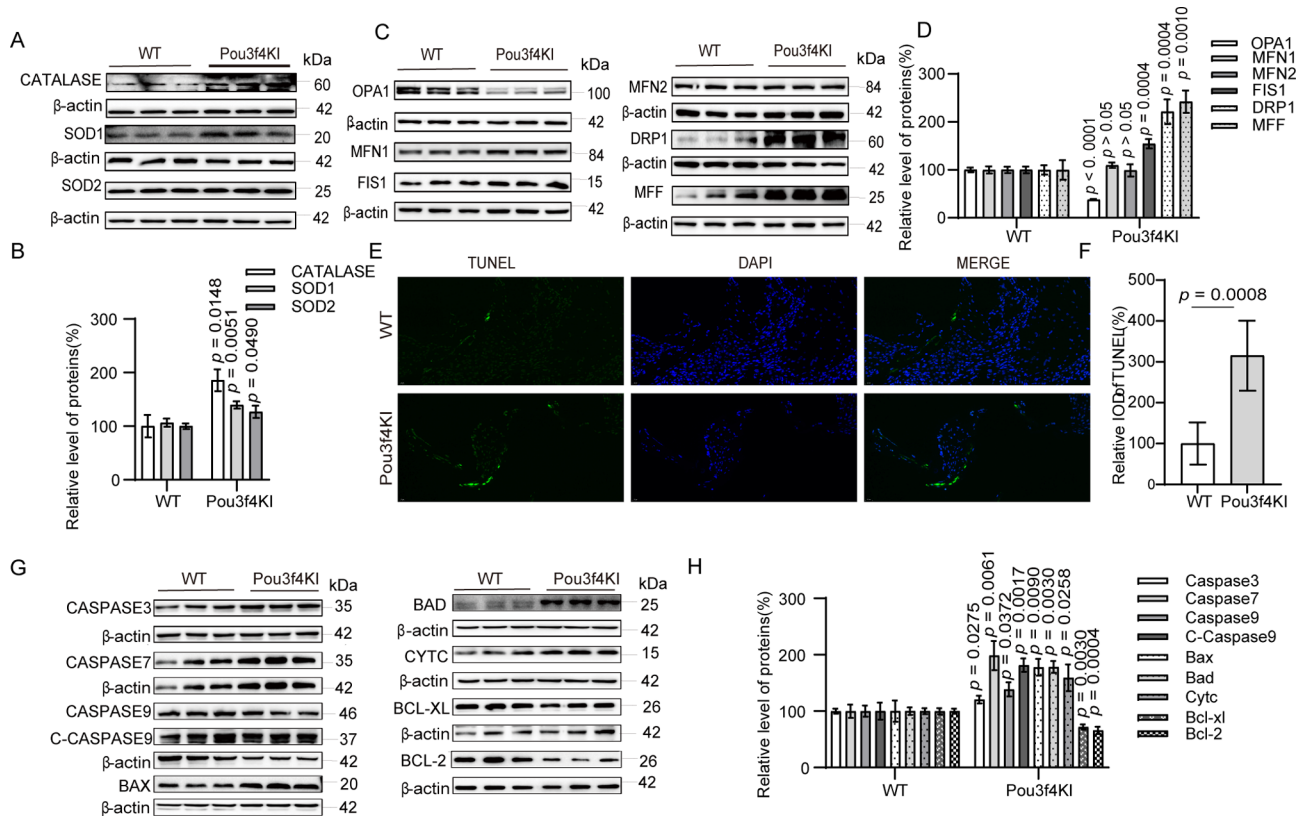


**Fig. 7** ROS Accumulation, Mitochondrial Dynamics, and Apoptosis. **(A, B)** Elevated levels of antioxidant enzymes (CATALASE, SOD1, and SOD2) in Pou3f4KI cochleae reflect increased mitochondrial ROS production due to the mutation. **(C, D)** Imbalanced mitochondrial dynamics show elevated fission-related proteins (DRP1, FIS1, MFF) and significantly reduced fusion-related protein (OPA1), suggesting excessive mitochondrial fission. **(E, F)** TUNEL staining shows a 3.1-fold increase in apoptotic cells in Pou3f4KI cochleae, predominantly in the spiral ligament, spiral limbus, modiolus, and basilar membrane. **(H, J)** Western blot analysis of apoptosis-related proteins demonstrates upregulated pro-apoptotic markers (CYTC, BAD, BAX, cleaved CASPASE9) and downregulated anti-apoptotic proteins (BCL-2, BCL-XL), strongly implicating the Pou3f4 mutation in apoptosis activation

genetic analysis, cell models and animal models, we provide insights into the molecular mechanisms underlying *POU3F4*-related hearing loss. *POU3F4* mutations are well-established contributors to X-linked non-syndromic hearing loss (DFNX2) [7], and this newly discovered mutation expands the phenotypic and genotypic spectrum of *POU3F4*-related hearing loss. The mutation resides within the highly conserved POU-homeo domain, a critical region for DNA binding and transcriptional regulation, underscoring its essential role in cochlear development.

Patient III-2 exhibited fluctuating hearing loss, contrasting with the typically progressive patterns observed in *POU3F4* mutations, such as the p.E294fs frameshift mutation described by Kandula et al., where the patient exhibited gradual worsening of mixed hearing loss [22]. The variability observed in III-2 could be influenced by multiple factors, including genetic modifiers and early compensatory mechanisms, which previous studies suggest contribute to intrafamilial and interfamilial differences in hearing loss severity among *POU3F4* mutation carriers [23]. Notably, patient III-2's early and continuous

monitoring captured these changes, emphasizing the importance of systematic hearing screening for timely intervention and a better understanding of hearing loss progression in *POU3F4* mutation cases. Interestingly, some Pou3f4KI mice also exhibited comparable fluctuations in hearing ability.

The p.E294G mutation impacts the POU-homeo domain, a critical region for DNA binding and cochlear development regulation. Structural analysis indicates that the substitution of glutamic acid to glycine at position 294 disrupts essential hydrogen bonds, potentially destabilizing this vital domain. This structural impairment may compromise the overall stability of the POU3F4 protein, further affecting its function in cochlear development.

In the family-derived immortalized lymphocyte cell lines we constructed, the c.881 A>G mutation significantly affected the stability and transcriptional levels of *POU3F4* mRNA. However, POU3F4 protein expression in the mutant cell lines (Hemi1, Hemi2) showed no significant changes, likely due to the inherently low expression of POU3F4 in lymphocyte cell lines. Further investigation revealed that the mutation altered the

subcellular localization of the POU3F4 protein, with *POU3F4*-MUT predominantly shifting from the nucleus to the cytoplasm, which may impact its function. Normally, *POU3F4* plays a crucial role in the nucleus, and this mislocalization may interfere with its functionality.

Several studies have investigated the impact of *POU3F4* mutations on its subcellular localization. It has been found that missense mutations, such as p.T211M and p.Q229R, affect the transcriptional activity of POU3F4 but do not significantly alter its subcellular localization. In contrast, frameshift mutations (such as p.Thr354Glnfs115, p.Leu317Phefs12, and p.Ile285Argfs43) and nonsense mutations (such as p.C327\*) result in the majority of POU3F4 being localized to the cytoplasm, indicating a disruption of nuclear localization [24–26]. Our study identifies the missense mutation p.E294G, which impairs both the stability and nuclear localization of POU3F4, shedding new light on its role in hearing development and subcellular localization mechanisms. In the *Pou3f4*KI mouse model, we observed a significant reduction in *Pou3f4* expression in the cochlea, which is linked to hearing impairment. Unlike most existing studies that focus on KO mice, our study is the first to use a p.E294G KI model, retaining partial POU3F4 function. This model better simulates human pathology and reveals novel phenotypic differences, including fluctuating hearing loss and mitochondrial dysfunction, which are not seen in KO models. This model better simulates human pathology and reveals novel phenotypic differences, including fluctuating hearing loss and mitochondrial dysfunction, which are not seen in KO models. These findings suggest that p.E294G may contribute to hearing loss via mechanisms distinct from complete loss of POU3F4. Taken together, the *POU3F4* c.881 A>G mutation likely causes developmental abnormalities linked to hearing impairment by affecting the stability and subcellular localization of *POU3F4* at the molecular level.

Histological analyses indicated significant dysplastic features, including hypoplasia of the modiolus, reduced tympanic scala size, and considerable cell loss in the stria vascularis, spiral ligament, and spiral limbus. These malformations are consistent with previous reports [27, 28].

Our study expands the understanding of *POU3F4* mutation effects by revealing significant reductions in both SGNs and hair cells in *Pou3f4*KI mice. This suggests that the *POU3F4* mutation contributes to auditory deficits by impairing key cell populations essential for cochlear function. Brooks et al. previously reported that the absence of *POU3F4* leads to significant SGN loss [29]. Additionally, *POU3F4* has been shown to support cochlear structural integrity, neuronal development, and connectivity [10, 11].

Interestingly, our study documented hair cell loss, which contrasts with previous knockout model studies. This discrepancy may reflect distinct phenotypic outcomes in the *Pou3f4*KI model. SEM analysis revealed notable cochlear morphological changes, including stereocilia misalignment in outer hair cells, significant loss of inner and outer hair cells, and disrupted filamentous bridges. TEM analysis further showed mitochondrial abnormalities in SGNs and myelinated fibers, such as swelling, deformation, and loss of cristae and membranes. Similarly, Minowa et al. reported mitochondrial defects in *Pou3f4*KO mice [30]. These findings suggest that *Pou3f4* mutations disrupt mitochondrial function, potentially compromising cell survival and cochlear integrity.

To further investigate the molecular mechanisms underlying hearing loss, reduced hair cells, SGNs, and mitochondrial dysfunction caused by *POU3F4*, we focused on that *POU3F4*, *POU2F1*, and *POU5F1* belong to the POU transcription factor family and share the conserved DNA-binding motif “TATGCAAT”. Using CHIP-seq data from the ENCODE database, we observed prominent binding peaks of POU2F1 and POU5F1 within the TFAM promoter region, suggesting that these transcription factors may regulate TFAM expression and subsequently influence mitochondrial function. Based on this, we examined the impact of POU3F4 on TFAM expression. In *Pou3f4*KI mice, TFAM expression was significantly reduced, indicating that the *POU3F4* mutation may impair mitochondrial function by down-regulating TFAM expression. Furthermore, overexpression of *POU3F4* (WT) in HEK293 cells led to a significant increase in TFAM expression, suggesting a potential regulatory relationship between *POU3F4* and mitochondrial function. As a critical factor linking the nucleus and mitochondria, *TFAM* is transcribed in the nucleus but functions within mitochondria to regulate the expression of mtDNA-encoded genes [31, 32]. These findings suggest that POU3F4 influences mitochondrial activity by regulating TFAM expression, thereby affecting mitochondrial biogenesis and function.

To further explore the molecular mechanism of *POU3F4* in cochlear function, we performed RNA sequencing on cochlear samples from *Pou3f4*KI and WT mice. We observed significant downregulation of mitochondrial-related pathways, alongside upregulation of calcium signaling and apoptosis pathways in the cochlea of *Pou3f4*KI mice. These findings suggest that *POU3F4* mutations may contribute to hearing impairment by modulating mitochondrial function, calcium ion concentration, and apoptosis, which can lead to cochlear cell damage and dysfunction.

To further investigate the impact of *Pou3f4* mutations on mitochondrial function, we performed Western blot,

BN-PAGE, and in-gel activity assays in the cochlea of Pou3f4KI mice. These analyses revealed a significant reduction in mitochondrial protein levels, assembly defects, and dysfunction of OXPHOS complexes. These defects, particularly in complexes I and IV, likely contribute to mitochondrial dysfunction in cochlear cells. Moreover, activity assays revealed significant decreases in the activity of OXPHOS complexes I, IV, and V. It further revealed that *Pou3f4* mutations disrupt both the assembly and functional activity of these complexes. This aligns with our RNA-seq data, which also indicated downregulation of mitochondrial-related pathways in Pou3f4KI mice, providing a comprehensive view of the molecular mechanisms underlying cochlear dysfunction.

The significant decrease in ATP levels suggests that *Pou3f4* mutations directly affect mitochondrial energy metabolism. Mitochondria are the primary site of ATP synthesis, and energy metabolism disorders are often associated with impaired oxidative phosphorylation due to defects in the assembly and activity of OXPHOS complexes I, III, IV, and V [33, 34].

Increased ROS production is typical of mitochondrial dysfunction. *POU3F4* is not expressed in hair cells, yet apoptosis was observed in hair cells. It has been reported that the survival of hair cells in the organ of Corti depends on the normal morphology and function of the StV [35]. Thus, *Pou3f4* mutations leads to StV dysfunction [28], which in turn leads to subsequent apoptosis of hair cells. Elevated ROS production can increase a vicious cycle of oxidative stress in the mitochondria, thereby worsening the damage to mitochondrial and cellular proteins, lipids, and nuclear acids [36].

The imbalance of mitochondrial dynamics was particularly significant in Pou3f4KI mice. These strongly indicated that the *POU3F4* c.881 A>G mutation regulated mitochondrial dynamics by promoting fission. The increase of mitochondrial division leads to a decrease in the ability of cells to cope with damage, especially in high-metabolic tissues such as the cochlea, and the imbalance of mitochondrial division will directly affect energy supply and cell survival [37].

Our findings provide strong evidence that the *POU3F4* c.881 A>G mutation induces significant cochlear cell apoptosis, particularly in the spiral ligament, spiral limbus, modiolus, and basilar membrane. This apoptotic cascade appears to be closely linked to mitochondrial dysfunction [38]. We observed a marked increase in mitochondrial fission, indicative of mitochondrial fragmentation, which is a key event in the initiation of intrinsic apoptosis [39]. Mitochondrial fragmentation is often accompanied by the release of pro-apoptotic factors such as Cytochrome C [40], which was significantly elevated in Pou3f4KI cochleae. These c.881 A>G mutation-induced alterations may lead to damaged or deficient inner ear

cells that are particularly vulnerable to neurodegeneration related to oxidative phosphorylation, thereby contributing to the development of hearing loss [41, 42].

In summary, we demonstrated that *POU3F4* mutations impair cochlear mitochondrial function by reducing *TFAM* expression, leading to increased ROS production and enhanced mitochondrial fission. These changes ultimately result in apoptosis in key cochlear regions, including the spiral ganglion, hair cells, spiral ligament, spiral limbus, stria vascularis (StV), and basilar membrane. This study provides critical experimental evidence for understanding the mechanisms of *POU3F4*-related hearing loss.

Further research is required to identify additional direct target genes regulated by *POU3F4* and to elucidate its precise functional network in cochlear development and physiology. Although this study integrates clinical cases, cell models, and KI mice to systematically analyze the p.E294G mutation, the limited number of familial cases prevents us from fully exploring the role of potential modifier genes that may influence the phenotype. Additionally, differences in cochlear structures between mice and humans suggest that the role of *POU3F4* may vary across species. Moreover, future studies will focus on investigating strategies to restore mitochondrial function, including pharmacological and genetic interventions. These efforts are part of our ongoing work to provide a stronger theoretical basis and practical strategies for the treatment of *POU3F4*-related hearing loss. Expanding patient cohorts and integrating human iPSC-derived cochlear organoids will be essential to further clarify the impact of the p.E294G mutation on human cochlear development.

## Conclusion

Our study demonstrates that the *Pou3f4* mutation leads to reduced *Tfam* expression, resulting in mitochondrial dysfunction, increased ROS production, and enhanced mitochondrial fission. These changes ultimately contribute to elevated apoptosis within the cochlea.

## Supplementary Information

The online version contains supplementary material available at <https://doi.org/10.1186/s12964-025-02133-y>.

Supplementary Material 1

## Acknowledgements

We thank Dr. Yanchun Ji, Dr. Feilong Meng, Dr. Qinghai Zhang, Ms. Meieriyi Yasheng, Ms. Huanhuan Zhang, Dr. Yunfan He and Dr. Gao Zhu in Center for Mitochondrial Biomedicine and Department of Ophthalmology, Zhejiang University School of Medicine, Yiwu, China, for their invaluable guidance and assistance during the experimental process. Their expertise and support have been instrumental in the successful completion of this work. We thank Ms. Guizhen zhu, Ms. Qin Han, Mr. Hang jun Wu, Ms. Yiping Lv in the Center of Cryo-Electron Microscopy (CCEM), Zhejiang University for their technical

assistance on (Transmission/Scanning Electron and Confocal Laser Scanning Microscopy). We thank the support from the recruited families for their invaluable cooperation and participation. We thank the animals used in this study for their contribution to advancing scientific knowledge.

#### Author contributions

Y.F.G., M.X.G. and B.C.X. designed the project. J.D. and P.P.B. performed patient workup. J.D., P.P.B. and C.C. drafted the manuscript. All authors critically revised and approved the final manuscript.

#### Funding

The financial support from the National Natural Science Foundation of China (No. 82160214, 32160149), the Cuiying Scientific and Technological Innovation Program of Lanzhou University Second Hospital (CY2023-MS-B08), Clinical Medical Center Construction Project of Gansu Province (21JR7RA434).

#### Data availability

The RNA-seq datasets generated and analyzed during the current study are not publicly available due to ongoing research. However, these datasets can be made available from the corresponding author upon reasonable request and with the permission of all relevant contributors.

#### Declarations

##### Ethics approval and consent to participate

The present study was approved by The Medical Ethics Committee of The Second Hospital of Lanzhou University. All informed consent was obtained from the subject(s) and/or guardian(s). Registry and the Registration No:2023 A-575. Animal Studies No: D2023-367.

##### Consent for publication

Not applicable.

##### Competing interests

The authors declare no competing interests.

##### Author details

<sup>1</sup>Department of Otolaryngology-Head and Neck Surgery, Lanzhou University Second Hospital, No. 82 Cuiyingmen, Lanzhou, Gansu 730030, PR China

<sup>2</sup>Center for Mitochondrial Biomedicine, Department of Ophthalmology, Zhejiang University School of Medicine, Yiwu, China

Received: 17 December 2024 / Accepted: 27 February 2025

Published online: 05 March 2025

#### References

- Fortnum HM, Summerfield AQ, Marshall DH, Davis AC, Bamford JM. Prevalence of permanent childhood hearing impairment in the united Kingdom and implications for universal neonatal hearing screening: questionnaire based ascertainment study. *BMJ*. 2001;323(7312):536–40.
- Watkin P, Baldwin M. The longitudinal follow up of a universal neonatal hearing screen: the implications for confirming deafness in childhood. *Int J Audiol*. 2012;51(7):519–28.
- Morton CC, Nance WE. Newborn hearing screening—a silent revolution. *N Engl J Med*. 2006;354(20):2151–64.
- Petersen MB, Wang Q, Willems PJ. Sex-linked deafness. *Clin Genet*. 2008;73(1):14–23.
- Del Castillo I, Morín M, Domínguez-Ruiz M, Moreno-Pelayo MA. Genetic etiology of non-syndromic hearing loss in Europe. *Hum Genet*. 2022;141(3–4):683–96.
- Bernardinelli E, Huber F, Roesch S, Dossena S. Clinical and molecular aspects associated with defects in the transcription factor POU3F4: A review. *Bio-medicines*. 2023;11(6).
- de Kok YJ, van der Maarel SM, Bitner-Glindzicz M, Huber I, Malcolm AP, Malcolm S, et al. Association between X-linked mixed deafness and mutations in the POU domain gene POU3F4. *Science*. 1995;267(5198):685–8.
- Sennaroglu L, Sarac S, Ergin T. Surgical results of cochlear implantation in malformed cochlea. *Otol Neurotol*. 2006;27(5):615–23.
- Sennaroglu L, Bajin MD. Incomplete partition type III: A rare and difficult cochlear implant surgical indication. *Auris Nasus Larynx*. 2018;45(1):26–32.
- Coate TM, Raft S, Zhao X, Ryan AK, Crenshaw EB 3rd, Kelley MW. Otic mesenchyme cells regulate spiral ganglion axon fasciculation through a Pou3f4/EphA4 signaling pathway. *Neuron*. 2012;73(1):49–63.
- Raft S, Coate TM, Kelley MW, Crenshaw EB 3rd, Wu DK. Pou3f4-mediated regulation of ephrin-b2 controls Temporal bone development in the mouse. *PLoS ONE*. 2014;9(10):e109043.
- Li P, Qian T, Sun S. Spatial architecture of the cochlear immune microenvironment in noise-induced and age-related sensorineural hearing loss. *Int Immunopharmacol*. 2023;114:109488.
- Miller G, Lipman M. Release of infectious Epstein-Barr virus by transformed marmoset leukocytes. *Proc Natl Acad Sci U S A*. 1973;70(1):190–4.
- Willott JF. Overview of methods for assessing the mouse auditory system. *Curr Protoc Neurosci*. 2006;Chap. 8:Unit8.21A.
- Fang QJ, Wu F, Chai R, Sha SH. Cochlear surface Preparation in the adult mouse. *J Vis Exp*. 2019(153).
- Xie L, Song XJ, Liao ZF, Wu B, Yang J, Zhang H, et al. Endoplasmic reticulum remodeling induced by wheat yellow mosaic virus infection studied by transmission electron microscopy. *Micron*. 2019;120:80–90.
- Livak KJ, Schmittgen TD. Analysis of relative gene expression data using real-time quantitative PCR and the 2(-Delta Delta C(T)) method. *Methods*. 2001;25(4):402–8.
- He Y, Zhu G, Li X, Zhou M, Guan MX. Deficient tRNA posttranscription modification dysregulated the mitochondrial quality controls and apoptosis. *iScience*. 2024;27(2):108883.
- Fiala GJ, Schamel WWA, Blumenthal B. Blue native polyacrylamide gel electrophoresis (BN-PAGE) for analysis of multiprotein complexes from cellular lysates. *JoVE*. 2011;48:e2164.
- Database JASPAR. The Open-Access Database of Transcription Factor Binding Profiles [Available from: <https://jaspar.elixir.no/>]
- Consortium EP. ENCODE: Encyclopedia of DNA Elements [Available from: <http://www.encodeproject.org/>]
- Kandula A, Schenker K. POU3F4 mutation and bilateral sensorineural hearing loss. *Pediatr Radiol*. 2024;54(10):1763–4.
- Han B, Cheng J, Yang SZ, Cao JY, Shen WD, Ji F, et al. Phenotype and genotype analysis of a Chinese family with prelingual X-linked hereditary hearing impairment. *Chin Med J (Engl)*. 2009;122(7):830–3.
- Parzefall T, Shvatzki S, Lenz DR, Rathkolb B, Ushakov K, Karfunkel D, et al. Cytoplasmic mislocalization of POU3F4 due to novel mutations leads to deafness in humans and mice. *Hum Mutat*. 2013;34(8):1102–10.
- Choi BY, Kim DH, Chung T, Chang M, Kim EH, Kim AR, et al. Destabilization and mislocalization of POU3F4 by C-terminal frameshift Truncation and extension mutation. *Hum Mutat*. 2013;34(2):309–16.
- Bernardinelli E, Roesch S, Simoni E, Marino A, Rasp G, Astolfi L, et al. Novel POU3F4 variants identified in patients with inner ear malformations exhibit aberrant cellular distribution and lack of SLC6A20 transcriptional upregulation. *Front Mol Neurosci*. 2022;15:999833.
- Phippard D, Lu L, Lee D, Saunders JC, Crenshaw EB 3. Targeted mutagenesis of the POU-domain gene Brn4/Pou3f4 causes developmental defects in the inner ear. *J Neurosci*. 1999;19(14):5980–9.
- Song MH, Choi SY, Wu L, Oh SK, Lee HK, Lee DJ, et al. Pou3f4 deficiency causes defects in otic fibrocytes and stria vascularis by different mechanisms. *Biochem Biophys Res Commun*. 2011;404(1):528–33.
- Brooks PM, Rose KP, MacRae ML, Rangoussis KM, Gurjar M, Hertzano R, et al. Pou3f4-expressing otic mesenchyme cells promote spiral ganglion neuron survival in the postnatal mouse cochlea. *J Comp Neurol*. 2020;528(12):1967–85.
- Minowa O, Ikeda K, Sugitani Y, Oshima T, Nakai S, Katori Y, et al. Altered cochlear fibrocytes in a mouse model of DFN3 nonsyndromic deafness. *Science*. 1999;285(5432):1408–11.
- Koh JH, Kim YW, Seo DY, Sohn TS. Mitochondrial TFAM as a signaling regulator between cellular organelles: A perspective on metabolic diseases. *Diabetes Metab J*. 2021;45(6):853–65.
- Scarpulla RC. Transcriptional paradigms in mammalian mitochondrial biogenesis and function. *Physiol Rev*. 2008;88(2):611–38.
- Harrington JS, Ryter SW, Plataki M, Price DR, Choi AMK. Mitochondria in health, disease, and aging. *Physiol Rev*. 2023;103(4):2349–422.
- Roger AJ, Muñoz-Gómez SA, Kamikawa R. The origin and diversification of mitochondria. *Curr Biol*. 2017;27(21):R1177–92.

35. Liu J, Bai Y, Feng Y, Liu X, Pang B, Zhang S, et al. ABCC1 deficiency potentiated noise-induced hearing loss in mice by impairing cochlear antioxidant capacity. *Redox Biol.* 2024;74:103218.
36. Schieber M, Chandel NS. ROS function in redox signaling and oxidative stress. *Curr Biol.* 2014;24(10):R453–62.
37. Zhang A, Pan Y, Wang H, Ding R, Zou T, Guo D, et al. Excessive processing and acetylation of OPA1 aggravate age-related hearing loss via the dysregulation of mitochondrial dynamics. *Aging Cell.* 2024;23(4):e14091.
38. Czabotar PE, Garcia-Saez AJ. Mechanisms of BCL-2 family proteins in mitochondrial apoptosis. *Nat Rev Mol Cell Biol.* 2023;24(10):732–48.
39. Zhang Z, Liu L, Wu S, Xing D. Drp1, Mif, Fis1, and MiD51 are coordinated to mediate mitochondrial fission during UV irradiation-induced apoptosis. *Faseb J.* 2016;30(1):466–76.
40. Taylor RC, Cullen SP, Martin SJ. Apoptosis: controlled demolition at the cellular level. *Nat Rev Mol Cell Biol.* 2008;9(3):231–41.
41. Keithley EM. Pathology and mechanisms of cochlear aging. *J Neurosci Res.* 2020;98(9):1674–84.
42. Ceriani F, Pozzan T, Mammano F. Critical role of ATP-induced ATP release for Ca<sup>2+</sup> signaling in nonsensory cell networks of the developing cochlea. *Proc Natl Acad Sci U S A.* 2016;113(46):E7194–201.

### Publisher's note

Springer Nature remains neutral with regard to jurisdictional claims in published maps and institutional affiliations.